Energy 147 (2018) 672–680

Contents lists available at ScienceDirect

Energy

journal homepage: www.elsevier.com/locate/energy

Thermo-element geometry optimization for high thermoelectric efficiency

Yongjia Wu [a], Jihui Yang [b], Shikui Chen [c], Lei Zuo [a, *]

[a] Department of Mechanical Engineering, Virginia Tech, Blacksburg, VA 24060, USA
[b] Department of Materials Science and Engineering, University of Washington, Seattle, WA 98195, USA
[c] Department of Mechanical Engineering, Stony Brook University, Stony Brook, NY 11794, USA

ARTICLE INFO

Article history:
Received 3 August 2017
Received in revised form
14 December 2017
Accepted 20 January 2018
Available online 4 February 2018

Keywords:
Compatibility factor
Efficiency
Thermoelectric generator
Selective laser melting

ABSTRACT

The figure of merit of thermoelectric materials is temperature dependent, and thus the local compatibility factor changes significantly along the thermo-element length. A local optimization method to maximize the efficiency of a function graded thermoelectric generator was proposed and discussed in this paper. By adjusting the cross-sectional area and segment's thickness, the reduced current equaled the compatibility factor of the material at every local thermo-element layer. This method can use the full potential of existing materials by maximizing the efficiency at every local thermo-element segment. For such a TEG working in a temperature range of 300–1100 K, the efficiencies of P-type segmented $Bi_{0.5}Sb_{1.5}Te_3$/BiSbTe/-PbTe/FeNbSb thermo-element and a N-type segmented $Bi_2Te_{2.79}Se_{0.21}$/$Bi_2Te_{2.9}Se_{1.1}$/SnSe/SiGe thermo-element were 25.70% and 21.73%, respectively, much higher than the conventional segmented thermo-elements. The overall efficiency of the device was more than 23.72%, making it a promising technology to harvest energy from medium and high-temperature industrial components. The optimized TEG can be fabricated by SLS/SLM technology.

Published by Elsevier Ltd.

1. Introduction

1.1. Segmented TEG for high energy conversion efficiency

Waste heat recovery from industrial process presents tremendous opportunities for energy savings across the industrial sectors, such as vehicle exhaust, power station, iron and steel manufacturing [1]. Thermoelectric energy conversion is a solid-state energy conversion technology using electrons and phonons as the virtual "working fluids". The efficiency of an ideal TEG is governed by its figure of merit ($ZT = \alpha^2 T/\kappa\rho$), where α is the Seebeck coefficient, ρ is the electrical resistivity, and κ is the thermal conductivity [2–6]. Generally, the efficiency of a TEG made by homogeneous materials is less than 10%, since no single material can achieve a high efficiency in a wide temperature range. It is believed that one of the most promising ways to increase the efficiency of the TEG is to fabricate inhomogeneous materials and structures, such as segmented/cascaded TEGs [7–9] and FGTM [6,10–12]. Currently, the best single-material-based TEG has an energy conversion efficiency of 16.4%, using skutterudites at a temperature difference of 500 K [13]. And the use of three-stage cascade-type TE modules could yield an overall energy conversion efficiency of 19.6% with the hot end temperature of 1200 K [9].

A typical segmented TEG (Fig. 1) consisting of low-, medium-, and high-temperature thermoelectric materials can take full advantage of the characteristics of different thermoelectric materials, thus achieving a high overall efficiency in a broad temperature range [7,8]. The concept to use the segmented design or FGTM to increase the overall efficiency of the device was first proposed by Ioffe et al. in the 1940s [14]. Since the 1970s, segmented RTGs, based on PbTe and SiGe, with efficiencies ranging from 3.0% to 7.0%, have been successfully applied in spacecraft as energy sources, providing heat and 2.7–290 W of electricity for the spacecraft during 5–10 year space missions [7]. The success of segmented TEGs in deep space application proved the potential they had in medium and high-temperature energy harvesting. The very essence of a segmented TEG design was to maximize local segment operating efficiency according to the local temperature [15,16]. In a broad sense, a FGTM can be regarded as a segmented TEG with infinite segments. In a FGTM, by changing the composite ingredients or the doping concentration along the thermo-element

* Corresponding author.
E-mail address: leizuo@vt.edu (L. Zuo).

https://doi.org/10.1016/j.energy.2018.01.104
0360-5442/Published by Elsevier Ltd.

Nomenclature

Symbols

T	Temperature (K)
Q	Heat flow (W/m^2)
P	Power output (W)
ZT	The figure of merit
J	Current density (A/m^2)
I	Current (A)
A	Area (m^2)
E	Electric field intensity (V/m)
L	Leg length (m)
κ	Thermal conductivity (W/(m K))
u	Reduced current (1/V)
s	Compatibility factor (1/V)
α	Seebeck coefficient (V/K)
ρ	Electrical resistivity (Ω m)
η	Efficiency

Subscript

P	P-type thermo-element
N	N-type thermo-element
H	Hot side
C	Cold side
r	Reduced efficiency
MAX	Maximum value

Abbreviation

TEG	Thermoelectric generator
FGTM	Functional graded thermoelectric material
RTG	Radioisotope thermoelectric generator
SPS	Spark plasma sintering
AM	Additive manufacture; SLS/SLM Selective laser sintering/melting

length gradually, the thermoelectric properties of the materials vary continuously [17–20]. The local carrier concentration of the thermoelectric material can be adjusted to obtain the desired transport properties, thus achieving high efficiency in a wide temperature range. In recent years, the academic field witnessed inspiring progress in FGTM for power generation applications [12,21]. However, the implementation of FGTM is still impeded by some practical difficulties associated with material fabrication, characterization, and modeling.

In homogenous thermoelectric materials, the properties of the materials do not change much in a relatively narrow temperature range, and thus the Thompson Effect can be neglected [22]. However, the properties of segmented TEGs vary significantly with temperature and the Thompson Effect has a significant influence on the system. In addition, the fabrication of segmented TEG requires more than simply piling up thermoelectric segments for different temperature intervals. The performance of segmented TEGs and FGTMs is closely related to the compatibility factor ($s = (\sqrt{1+ZT}-1)/(\alpha T)$), which varies with temperature appreciably. When the compatibility factors differ by a factor of 2 or more, the maximum efficiency can in fact decrease by segmentation [23]. Only when the reduced current ($u = J\nabla T$) is equal to s, will the local thermoelectric material achieve the maximum efficiency [16]. However, since the electric current on the thermo-element is constrained by the cross-sectional area of the TEG, the change in u is limited. The difference between u and s for the local thermoelectric segment makes the actual efficiency of a TEG less than the theoretical peak value.

1.2. Literature review

Conventionally, attempts to improve the economic viability of TEGs concentrated primarily on increasing their figure of merit (ZT). Though considerable effort has been put into this area since the 1990s when Hicks and Dresselhaus proposed that low dimensional thermoelectric materials might enhance the ZT value by several times [24,25], materials with good and stable performance are still in exploration. The very essence of thermoelectric material research is to reduce the thermal conductivity while preserving the electrical conductivity. Many new concepts were examined in the past decade, like matrix and precipitates band alignment, all-length-scale hierarchical architectures, modulation doping, etc. A lot of progress was made in both improving the performance of existing materials and exploring new materials. The ZT of some materials, like SnSe (n-type), and PbTe-SrTe (p-type), were reported to be higher than 2.0 in a wide temperature range. Comprehensive reviews summarizing the most recent state-of-the-art approaches to designing high-performance thermoelectric materials can be seen in Refs. [26–29].

Another attempt to improve their economic competitiveness is

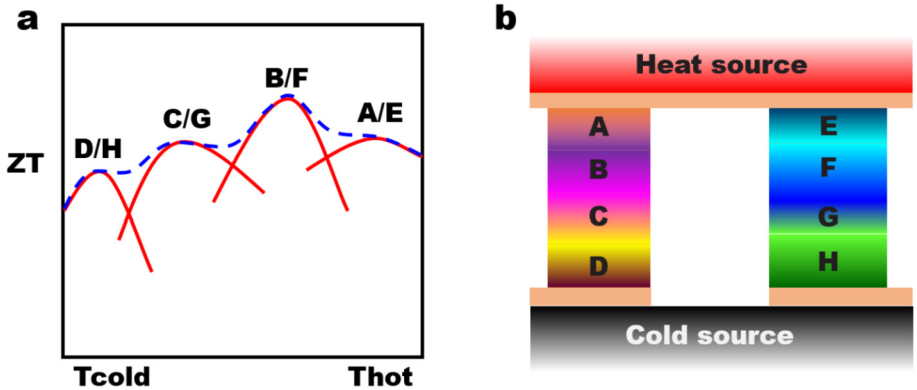

Fig. 1. **(a)** Segmented TEG using different TE materials to achieve highest averaged ZT value in a broad temperature range; **(b)** A segmented TEG design using these materials for high device efficiency.

to make the best of materials commercially available [30]. Thermo-elements, limited by the manufacturing processes available now, are rectangular or cylindrical in shape. As the cross-section of the thermo-elements is constant, the reduced current density cannot change with the compatibility accordingly, and thus the efficiencies of the thermoelectric materials are not fully explored. The compatibility mismatch has been a practical problem that hinders the further improvement of efficiency of TEG device. To conduct efficiency analysis of the segmented TEG relys on accurate thermal model. The most widely used analytical model to analyze the performance of the TEG module is the ideal one-dimensional model [18]. However, this model was accused of being poor accuracy as it neglected the thermal resistance, heat leakage, and Thompson effect. More accurate models can be seen in Refs. [18,22,31–37] to analyze the performances of TEGs working in different scenarios. Because the Thompson term introduces nonlinearity in the thermodynamic governing equation, to obtain the exact analytical solution for the TEG is difficult. Analytical modeling by Sahin et at [38,39] found it was possible to increase the conversion efficiency by adjusting the geometry of the thermo-element. They calculated the efficiency of the thermo-elements with different geometry shapes and compared the results with the rectangle shaped thermos-elements. However, it was still obscure what was the best geometry shape for the highest energy conversion efficiency. Numerical method was widely used as it can take account all the effects into accounts and was of excellent geometry adaptability [40]. However, geometry optimization through numerical method can be complicated and time-consuming, because all the factors were inter-related. Snyder [16,41] proposed a novel spreadsheet method to optimize the performance of a segmented TEG with rectangle geometry shape. This method, by separating the internal variables and properties from the external ones, allows one to compare the exact local efficiency with the ideal efficiency. In this paper, a similar spreadsheet method was adopted to analyze the optimal geometry shape of each local thermoelectric segment.

We have selected three thermoelectric material segments for each of the thermoelectric legs in the device to balance the performance gains and system complications. The materials we choose for the N-type leg are $Bi_2(TeSe)_3$-based for the low-temperature range [42,43], SnSe for the intermediate temperature range [44], and SiGe for the high-temperature range [45]. On the P-type side, the material choices for the low, intermediate, and high temperature range are $(BiSb)_2Se_3$-based [46,47], PbTe [48], and FeNbSB [49], respectively. These materials are chosen for their high ZT values and similar compatibility factors at the interfaces. In addition, in order to realize the maximum average ZT, the low-temperature ends of both elements have two compositions, but within the same family of materials, hence we consider these single segments. By changing the thickness and cross-sectional area of each local thermoelectric segment, the compatibility mismatch problem in the segmented TEG construction is eliminated. This optimized segmented TEG can make the best of the existing thermoelectric materials. The relatively complex geometry structure of the thermo-elements will introduce extra difficulty in fabrication. It is not practical to use the conventional methods, such as hot pressing, SPS, and Bridgeman method to fabricate this kind of TEG module. SLS/SLM, a higher temperature AM method, is proposed to be a good choice for the manufacturer.

2. Mathematical model

In a thermoelectric material, thermal energy is converted to electricity based on the Seebeck, Peltier, and Thompson effects. The efficiency of a general TEG device is traditionally described in terms of system parameters such as hot- and cold-side temperature, length and area of thermo-element, and load resistance. Because of the nonlinearity introduced by the Thompson heat term [22,33], in only the most simplified cases (e.g., temperature-independent thermoelectric properties), can the efficiency of the TEG device be computed analytically. In a FGTM/segmented TEG, all the properties (e.g., Seebeck coefficient, electrical resistivity, thermal resistivity) are highly temperature dependent. In most case, it is impossible to obtain the analytical solutions. In this paper, a spreadsheet method [16,18,41] proposed by Snyder is used to optimize the geometry shape of the thermo-element. By taking Fourier's heat conductivity, Peltier Effect, Thompson Effect, and Joule heat into account, the analysis aimed at accurately predicting the possible highest efficiency of the TEG through geometry optimization using the most advanced materials. The thermo-element is divided into many segments mathematically. For each segment, the cross-sectional area and the length are optimized, thus achieving the peak efficiency at every temperature interval.

The electric current density through the thermo-element is

$$J = \frac{I}{A} \tag{1}$$

The generated electrical field in thermoelectric material is caused by Seebeck Effect ($E_1 = \alpha\nabla T$) and counteracted by Ohm's law ($E_2 = -\rho J$). The electrical field in the thermo-element at a given position is described as

$$E = \alpha\nabla T - \rho J \tag{2}$$

At the cross-section, the heat transported is given by

$$Q = \alpha TJ + \kappa\nabla T \tag{3}$$

where the first term is the heat absorbed by the Peltier Effect and the second term is the heat transferred according to the Fourier's law.

The electric power density (power generated per volume) is expressed as

$$P = EJ \tag{4}$$

According to the energy conservation law, the divergence of heat flux should be compensated by the source term from Joule heat; then the electrical power density can be rewritten as

$$P = \nabla Q \tag{5}$$

Substituting Eq. (3) into Eq. (5) yields

$$P = \nabla(\alpha TJ + \kappa\nabla T) = \nabla T\left(\frac{d\alpha}{dT}\cdot TJ + J\alpha\right) + \nabla J\cdot T\alpha + \nabla(\kappa\nabla T) \tag{6}$$

In Eq. (6), Effect $\left(\frac{d\alpha}{dT}\cdot T\right)$ is the Thompson coefficient. Using the sign presented in Fig. 2, a sign computation finds that the power density ($P = -\rho J^2$) is negative. Here the electric current flux ($\nabla J \neq 0$) is a function of position. Plugging Eq. (4) into Eq. (6), yields the steady state thermodynamic governing equation

$$\nabla(\kappa\nabla T) = -\nabla T\frac{d\alpha}{dT}\cdot TJ - \nabla J\cdot T\alpha - \rho J^2 \tag{7}$$

The relative current density (u) [41], which is the ratio of the electric current density (J) to the heat flux by conduction $\kappa\nabla T$, is introduced to simplify the calculation, which is described as

$$u = \frac{J}{\kappa\nabla T} \tag{8}$$

Then the heat flux through the cross-section of the thermo-element (Eq. (3)) and electric power density (Eq. (4)) in term of u

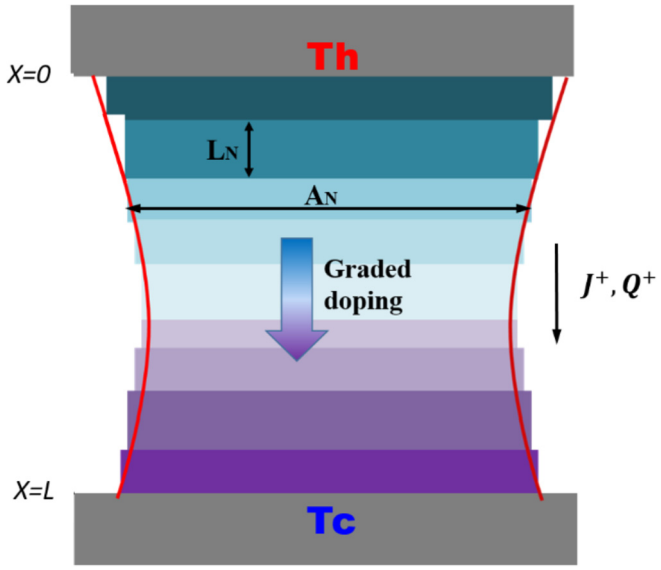

Fig. 2. Mathematical segments of a single thermo-element. The direction of positive variables is shown relative to the hot- and cold-ends.

then can be rewritten as

$$Q = (1 + \alpha u T)\kappa \nabla T \tag{9}$$

$$P = (\alpha - \rho u \kappa)\kappa \nabla T^2 \tag{10}$$

The variation of u is governed by Eq. (7), which is a function of temperature. For the one-dimensional problem, the variation of u in term of temperature can be expressed in term of position.

$$\frac{du}{dT} = \frac{du}{dx} \cdot \frac{1}{\nabla T} \tag{11}$$

Differentiating Eq. (8) over x on both sides yields variation of u in term of position.

$$\frac{du}{dx} = \frac{dJ}{dx} \cdot \frac{1}{\kappa \nabla T} - \frac{J}{(\kappa \nabla T)^2}(\nabla(\kappa \nabla T)) \tag{12}$$

Plugging Eqs. (7) and (11) into Eq. (12), the u value is constrained by the updated thermodynamic governing equation.

$$\frac{du}{dT} = u^2 T \cdot \frac{d\alpha}{dT} + \rho u^3 \kappa - \frac{dA}{dT} \cdot \frac{(1 + uT\alpha)u}{A} \tag{13}$$

The local segment efficiency is defined as the power produced divided by the heat flux going through the local segment. For a small segment, the power generated per area is given by Pdx, and the efficiency of the local thermoelectric segments is neatly given by

$$\eta_{local} = \frac{Pdx}{Q} \tag{14}$$

Plugging Eqs. (9) and (10) into Eq. (14) yields

$$\eta_{local} = \left(\frac{dT}{T}\right) \cdot \left(\frac{u(\alpha - u\rho\kappa)T}{u\alpha T + 1}\right) = \eta_C \cdot \eta_r \tag{15}$$

where the η_C is the Carnot efficiency, and η_r is the reduced efficiency. To achieve the highest efficiency, $\partial \eta_r / \partial u = 0$, the reduced current should equal to

$$u_{MAX} = s = \frac{\sqrt{1 + ZT} - 1}{\alpha T} \tag{16}$$

The s in Eq. (16) is the so-called compatibility factor of the local thermoelectric segment, which is derived from the temperature-dependent materials properties, such as α, ρ, κ. Thus s, like ZT, is independent from device geometry or the alteration of electric or thermal currents. The largest η_r is given by

$$\eta_{r\_MAX} = \frac{\sqrt{1 + ZT} - 1}{\sqrt{1 + ZT} + 1} \tag{17}$$

Only when $u = s$, will each TEG segments achieve the peak efficiency in the local position. For conventional TEG, the cross-section is constant, Eq. (13) can be simplified as

$$\frac{du}{dT} = u^2 T \cdot \frac{d\alpha}{dT} + \rho u^3 \kappa \tag{18}$$

Once u is selected at one point, it cannot be adjusted in a thermo-element to follow the temperature variation of s, because the variation of u is fixed by the thermodynamic governing equation (Eq. (18)). Conveniently, the variation of u ($u = \frac{J}{\kappa \nabla T}$) within a conventional thermoelectric leg is typically small, since all segments in a thermoelectric element are electrically and thermally in series, current J is the same and the thermal conductivity k varies little along the thermo-element with the same material. However, the material property s can vary significantly along the thermos-element, even in a same material working at a large temperature difference. So u and s cannot be equal at more than a few isolated points. The difference between u and s let the efficiency of the thermos-electric device deviate from the maximum efficiency that the device can achieve. The strategy to maximize the efficiency of the TEG device is to make the u close to the s at every thermo-electric segment.

Known from Eq. (13), if the cross-section is not a constant, the reduced current can be adjusted by tuning the shape of the thermo-element. Rearranging Eq. (13) varies the cross-sectional area in temperature.

$$dA = \frac{\left(u^2 T \cdot \frac{d\alpha}{dT} + \rho u^3 \kappa - \frac{du}{dT}\right) A dT}{(1 + uT\alpha)u} \tag{19}$$

After the cross-sectional area is obtained, plugging Eq. (8) into Eq. (17), the cross-sectional area is related to temperature gradient by

$$A = \frac{\alpha I T}{\kappa \nabla T\left(\sqrt{1 + ZT} - 1\right)} \tag{20}$$

Rearranging Eq. (20), the length of each segment is given by

$$dx = \frac{\kappa A dT\left(\sqrt{1 + ZT} - 1\right)}{\alpha I T} \tag{21}$$

By tuning the length of each TEG segment, the value of u can be calibrated to the desired value. Once the geometry of each segment is obtained, the length, electrical resistance, and voltage output of the thermos-element can be obtained by integrations

$$L = \int dx \tag{22-1}$$

$$R = \int \rho A dx \tag{22-2}$$

$$V = \int \alpha dT \tag{22-3}$$

Dividing the thermo-element into numerous segments, according to reference [41,50], the overall efficiency of the single thermo-element (P or N-type) can be expressed as

$$\eta_{series} = 1 - exp\left(- \int \frac{\eta_{local}}{T} dT \right) \tag{23}$$

The cross-sectional areas at the hot- and cold-ends of the P- and N-type thermo-elements are selected as the reference areas for the two thermos-elements respectively. The ratio of the reference areas of the P-type thermo-element to the N-type thermo-element can be adjusted to make sure that the length of the P, N-type thermo-elements are the same.

$$L_P = L_N \tag{24}$$

For two thermoelectric elements thermally in parallel, the combined efficiency is an average of the efficiency of both generators weighted by the heat flow through each thermo-element. The efficiency of the TEG device finally arrives as

$$\eta_{TEG} = \frac{\eta_N Q_N + \eta_P Q_P}{Q_N + Q_P} \tag{25}$$

To implement the optimization approach, the temperature operation range (300–1100 K) is divided into temperature intervals at a step of 10 K. The geometries of the local thermos-element segments are then optimized according to the local temperature. In each small temperature interval, the material properties are assumed to be the average values of properties at *Th* and *Tc*. The spreadsheet method is presented in Fig. 3.

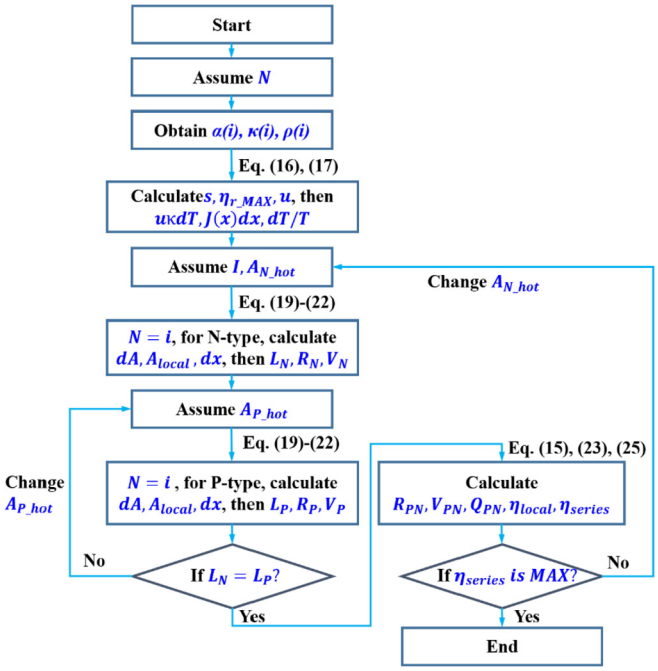

Fig. 3. The procedures of the TEG geometry optimization method.

3. Results and discussion

3.1. The conventional thermo-element

The materials we selected are $Bi_2Te_{2.79}Se_{0.21}$/$Bi_2Te_{2.9}Se_{1.1}$/SnSe/SiGe for N-type thermo-element and $Bi_{0.5}Sb_{1.5}Te_3$/BiSbTe/PbTe/FeNbSb for P-type segmented. The thermoelectric properties (α, ρ, κ) are functions of temperature [38–45]. At the interface between two different materials, the thermo-electric properties (e.g., *ZT*) are discontinuous (Fig. 4).

In the computation, by combining the zero Thomson effect solution ($d\alpha/dT = 0$) with the zero resistance solution ($\rho k = 0$) [41,51], the differential Eq. (18) can be approximated as follows

$$\frac{1}{u_n} = \frac{1}{u_{n-1}} \sqrt{1 - 2u_{n-1}^2 \overline{\rho k} \Delta T} - \overline{T} \Delta \alpha \tag{26}$$

where operator $\Delta T = T_n - T_{n-1}$, $\Delta\alpha = \alpha(T_n) - \alpha(T_{n-1})$, and $\overline{\rho k}$ and $\overline{T}$ means the average of ρk and T between T_n and T_{n-1}. At the interface between two materials, the discontinuous change in u can be correctly calculated using $\Delta u = u^2 T \Delta\alpha$ that is simplified from Eq. (18). Using an initial, the reduced current (u) can be calculated using Eq. (26). By varying the initial u condition, the maximum efficiency can be calculated from Eqs. (15) and (23). In this design, the optimal initial u for the P- and N-type thermo-elements are 3.65 and $-1.16\ V^{-1}$.

The reduced currents (u) and compatibility factors (s) of P- and

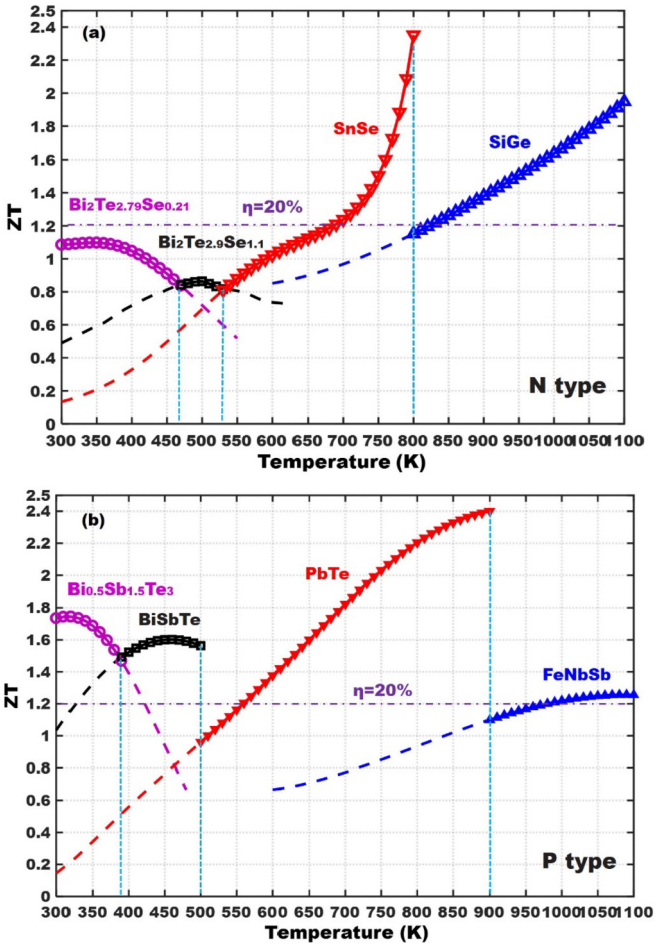

Fig. 4. Variation of ZT values with temperature for **(a)** N- and **(b)** P-type thermoelectric materials.

N-type thermos-elements change drastically with temperature, as shown in Fig. 5. For the traditional thermo-element with the constant cross-section design, the reduced current doesn't change much within this temperature range. However, the compatibility factor differs more significantly. Because the reduced current differs with the compatibility factor, as shown in Fig. 5, the actually reduced efficiency of the thermo-element is lower than the maximum reduced efficiency (Fig. 6).

The desired thermo-element length (from Eq. (21) and (22)) can be calculated by $l = \int_{T_c}^{T_h} ukdT/J$. If the electric current density is 5.0 A/mm^2 and the cross-sectional area of the N-type thermo-element is 100 mm^2, the corresponding thermo-element length of the N-type thermo-element is 14.3 mm. The length of the P-type thermo-element should be equal to that of the N-type one, thus the cross-sectional area of the N type thermo-element should be adjusted accordingly. For this case, the cross-sectional area and the electric current density of the P-type thermo-element are 13.4 mm^2 and 37.3 A/mm^2, respectively. For the P- and N-type thermo-elements, the energy conversion efficiencies are 22.9% and 12.2%, respectively. Known from Fig. 4, the average ZT for the P- and N-type thermo-elements are about 1.2, the expected efficiency should be about 20.0%. For P type thermo-element, the actual efficiency does not differ too much with the expected value. However, for the N type thermos-element, the actual efficiency (12.2%) is far below the desired value (20%). As explained in Ref. [23], if the compatibility factor differ by a factor of 2 or more, the maximum efficiency can be decreased by segmentation. The heat fluxes, calculated using Eq. (9), enter the hot ends of the P- and N-type thermo-element are 2.56 and 5.78 W, respectively. Substituting the heat fluxes into Eq. (25), the overall efficiency of the conventional thermoelectric device is 15.48%.

3.2. The optimized thermo-element

As mentioned above, to achieve the maximum reduced efficiency, u should be as close to s as possible. For traditional thermo-element, restricted by the constant cross-section, u cannot change accordingly with the s. The substantial difference between u and s makes the actual efficiency deviate far less than the maximum value. If the cross-section and segment length can vary according to the local temperature, the TEG can achieve the theoretical maximum efficiency. The mismatch problem of compatibility factor that restricts the combinations of different thermoelectric materials, in turn, can be solved.

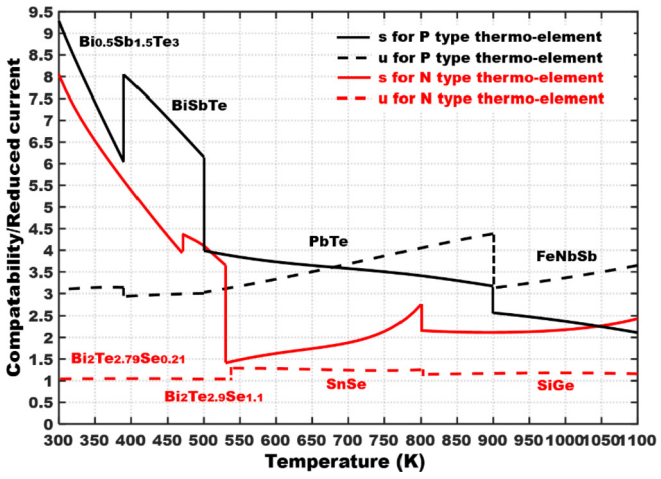

Fig. 5. Variation of u and s with temperature for the segmented TEG.

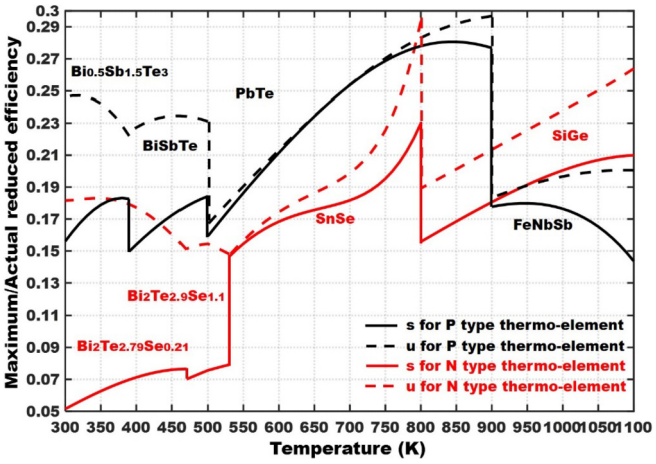

Fig. 6. Variation of η_{r_Max} and η_r with temperature for the segmented TEG.

The detailed procedures of the optimization method are described in Fig. 3. The key idea underneath this scheme is to let the reduced current equal to the compatibility factor at every local segment. To achieve this, the cross-sectional area and the length of thermoelectric segments should be adjustable. The reference cross-sectional area of the N-type thermo-element used for this calculation is 100 mm^2, and the electric current density is 5.0 A/mm^2. Fig. 7 showed the results calculated by the optimization method, including the cross-sectional areas, accumulated length and efficiency (from the hot ends) for P- and N-type thermo-elements. To alleviate the possible difficulty in fabrication, the cross-sectional area between two different materials is continuous. As we can see from Fig. 7(a), even in the same material, the cross-sectional area varies significantly with the temperature. As for the accumulated length, it does not increase strictly linearly with the temperature (Fig. 7(b)). The variations of the cross-sectional area respect to length of the thermo-elements are depicted in Fig. 8. For the optimized P-type thermo-element, the cross-section area decreases with length gradually. The cross-sectional area at the hot end is about 3 times of that at the cold end. For the N-type thermo-element, near the cold end, the cross-sectional area varies significantly along the thermo-element length. However, near the hot end, the cross-sectional area is nearly uniform. The variations of the cross-sectional area introduce extra difficult in manufacture, which requires fabrication method with excellent material and geometry flexibility.

Using the efficiency optimization method, the maximum efficiencies achievable for the P- and N-type thermo-elements are 25.70% and 21.73% (Fig. 7(c)), respectively. Computed using Eq. (9), the heat fluxes entering the hot ends of the P- and N-type thermo-elements are 3.55 and 3.52 W, respectively. And the overall efficiency of the TEG device constructed by these two thermo-elements is 23.72%. When compared with the efficiencies obtained using the traditional thermo-elements, both the efficiencies of the optimized P- and N-type thermo-elements increase significantly, especially for the N-type one. The efficiency of the N-type thermo-element increase from 12.2% to 21.73%, while the efficiency of the P-type thermo-element increases from 22.9% to 25.70%. In a scenario where s varies smoothly, the conventional TEG works well (like the P-type thermo-element). However, in other cases, the averaging method will lead to the large difference (like the N-type thermo-element) [18]. This phenomenon was also mentioned by Snyder in Ref. [18], where he explained why segmentation of $(AgSbTe_2)_{0.15}$ $(GeTe)_{0.85}$ (TAGS) with SnTe or PbTe had produced little extra power [52], but using filled skutterudite would increase

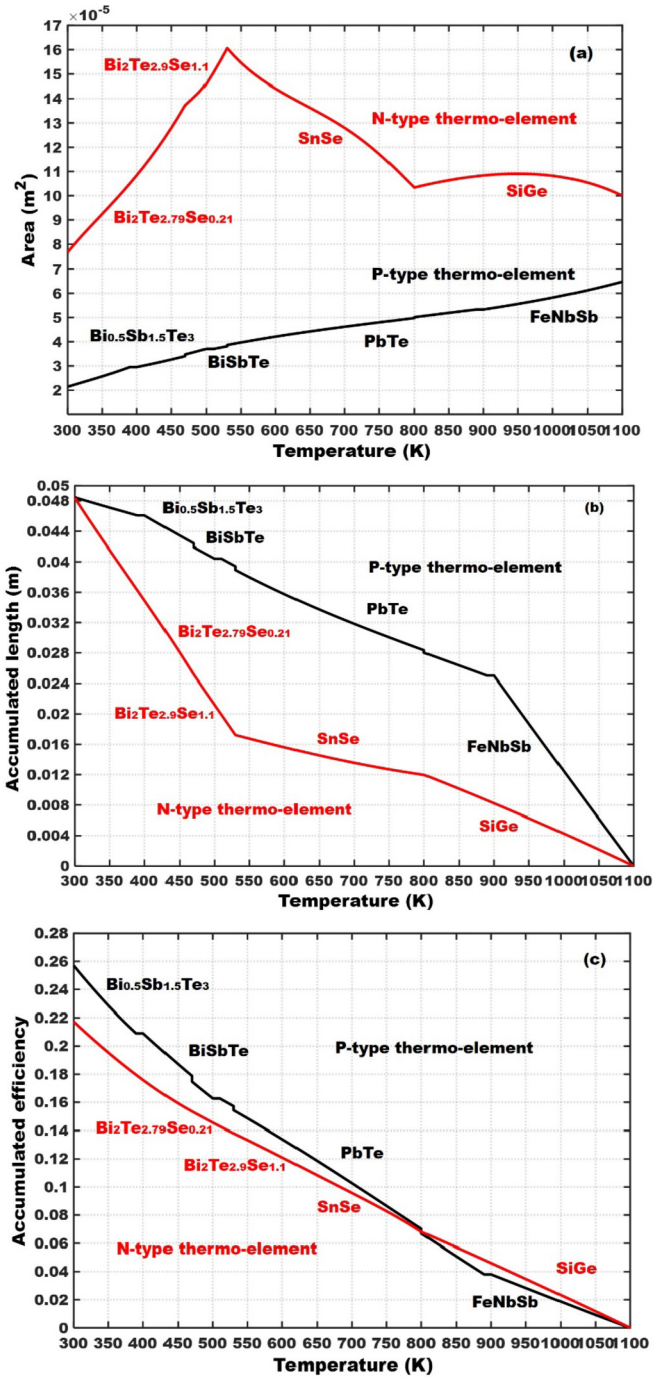

Fig. 7. Variations of **(a)** the cross-sectional areas, **(b)** accumulated lengths and **(c)** efficiencies (from the hot ends) with temperature for P- and N-type thermo-elements.

the efficiency from 10.5% to 13.6% [16]. For segmented TEG or FGTM working in significant temperature difference, the combination of different thermoelectric materials to construct a high-performance TEG, constrained by the compatibility factor mismatch, are limited. However, for the design with variable thermo-element cross-section, the reduced current can be adjusted to match the compatibility factor conveniently. Thus there is no requirement on the material's compatibility factor. The only criterion that matters in constructing a high-performance TEG is *ZT* value.

Conventionally, a TEG is fabricated by traditional methods, such as Bridgman, SPS, hot press, and thermal spay methods. Because of

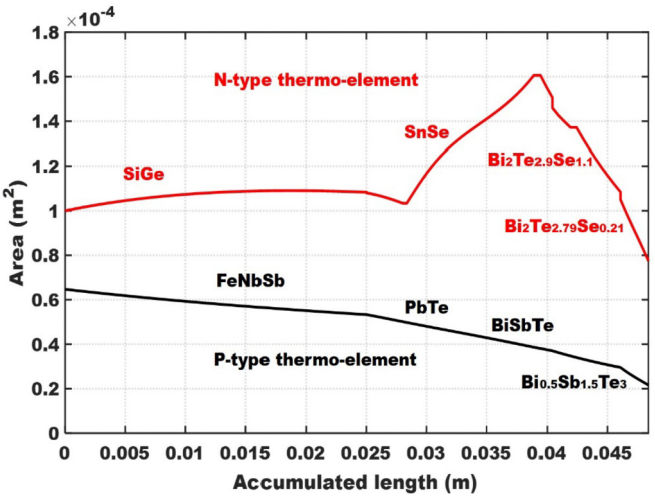

Fig. 8. Variations of the cross-sectional areas with the accumulated lengths for P- and N-type thermo-elements.

the complex geometry of segmented thermo-element, it is not convenient to implement this optimization method using the conventional fabrication methods. Recently, several groups [53–56] around the world did some preliminary work to test the possibility of sintering semiconductor thermoelectric material using SLS/SLM. The thermoelectric properties varied according to the composition, as expected, demonstrating the feasibility of laser melting as a rapid synthesis tool for thermoelectric compounds. As 3D AM methods (e.g., SLS/SLM) fabricate devices layer by layer with a thickness of 1–200 μm, it is convenient to change the stoichiometric proportions and geometry structures during processing. 3D printed TEG removes the need to assemble this fairly complex device piece by piece, instead of allowing it to be efficiently printed using a single machine (Fig. 9).

The performance of the TEG is determined mainly by the ZT value of the thermoelectric material. There are many reasons to believe that the ZT value fabricated by SLS/SLM, though might a bit smaller than corresponding super lattice well synthesized [57] (which has very high cost and low throughput), will be competitive to that fabricated by a conventional method or even higher. The SLS/SLM method removes the energy and time-consuming melting and quenching processes in the conventional fabrication, giving it a tremendous economic advantage over conventional methods. According to the recent research done by Tang et al. [56], the n-type $Bi_2Te_{2.7}Se_{0.3}$ fabricated by SLM manufacturing achieved an averaged ZT of ~0.7 in the temperature range of 300–550 K, which is comparable to that of the corresponding material commercially available. When integrated with technologies such as hyper-scale phonon scattering [3], graded doping [17], geometry optimization (described in the section above), and nano-structuring [4], the performance of the thermoelectric materials fabricated by SLS/SLM can be even enhanced. The wavelengths of the current carriers are much smaller than the phonons, the wavelength mismatch between the phonons and electrons makes it is possible to maintain the electrical conductivity with carefully selected size and concentration of nanoparticles. Other potential nano-particles after band alignment checking can be added into the matrix material acting as a carrier filtering layer [58]. Thus the Seebeck coefficient of the resulted deposited materials will be increased, and the bipolar thermal conductivity will be restricted [59]. The ZT of the final nanocomposites can be maximized by maintaining or even enhancing the electrical transport properties but also further decreasing the thermal conductivity [60]. Meanwhile, by removing

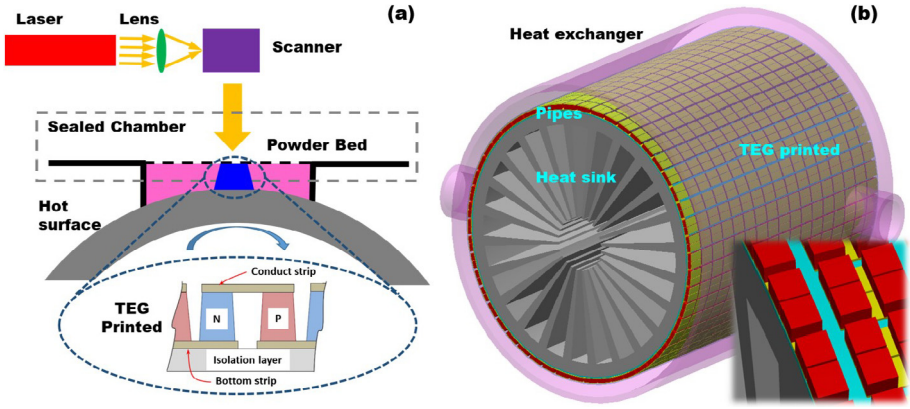

Fig. 9. **(a)** Depositing TEG device directly on industrial components using SLS/SLM; **(b)** The concept of printing TEG on vehicle exhaust pipe.

the time-consuming melting and cutting processing in the conventional methods, the time and energy to product a TEG module using 3D printing can be greatly reduced, resulting in a significant cut in the cost. Using SLM/SLS and integrating with this optimization strategy, we might develop a game changing fabrication method for cheap and high performance TEGs.

4. Conclusions

In this paper, a local optimization scheme based on a reduced current analysis is introduced to increase the efficiency of segmented TEG device. By calibrating the cross-sectional area and thickness of each segment, the reduced current matches to the compatibility factor of the thermoelectric materials at every point along the thermo-element, thus achieving the highest overall efficiency of TEG device.

1) A conventional N-type segmented $Bi_2Te_{2.79}Se_{0.21}/Bi_2Te_{2.9}Se_{1.1}$/SnSe/SiGe thermo-element and a P-type $Bi_{0.5}Sb_{1.5}Te_3$/BiSbTe/PbTe/FeNbSb thermo-element working a temperature range of 300–1100 K are established. The efficiency of the P- and N-type thermo-elements are 22.9% and 12.2%, where the efficiency of N-type thermo-element is far less than the expected value predicted by the averaging method.
2) An optimization method is used to construct the P- and N-type thermos-elements by adjusting the geometry shape of each segment. The efficiency of the N-type thermo-element increase from 12.2% to 21.73%, while the efficiency of the P-type thermo-element increases from 22.9% to 25.70%. The optimized thermo-elements have significantly higher efficiency than the traditional ones because of removing the constraints in the compatibility factor.
3) The cross-sectional area varies along the thermo-element length, making it impossible to be fabricated by the conventional processes. SLS/SLM is proposed to be a workable and economical way to fabricate this TEG device. Further work can be done to try this idea using SLS/SLM. The life cycle of this device will be examined, too.

Acknowledgments

The authors gratefully acknowledge financial support from the US National Science Foundation via Grant #1508862 and #1529842. Thank Jackson A. Klein in Virginia Tech for helping with the manuscript preparation.

References

[1] Manufacturing energy and carbon footprints (2010 MECS). In: Department of Energy U, editor.2010.
[2] Zhao LD, Lo SH, Zhang YS, Sun H, Tan GJ, Uher C, et al. Ultralow thermal conductivity and high thermoelectric figure of merit in SnSe crystals. Nature 2014;508(7496). 373-+.
[3] Biswas K, He JQ, Blum ID, Wu CI, Hogan TP, Seidman DN, et al. High-performance bulk thermoelectrics with all-scale hierarchical architectures. Nature 2012;489(7416):414–8.
[4] Poudel B, Hao Q, Ma Y, Lan YC, Minnich A, Yu B, et al. High-thermoelectric performance of nanostructured bismuth antimony telluride bulk alloys. Science 2008;320(5876):634–8.
[5] Nakpathomkun N, Xu HQ, Linke H. Thermoelectric efficiency at maximum power in low-dimensional systems. Phys Rev B 2010;82(23).
[6] Dashevsky Z, Shusterman S, Dariel MP, Drabkin I. Thermoelectric efficiency in graded indium-doped PbTe crystals. J Appl Phys 2002;92(3):1425–30.
[7] El-Genk MS, Saber HH, Caillat T. Efficient segmented thermoelectric unicouples for space power applications. Energy Convers Manag 2003;44(11):1755–72.
[8] El-Genk WS, Saber HH. High efficiency segmented thermoelectric unicouple for operation between 973 and 300 K. Energy Convers Manag 2003;44(7):1069–88.
[9] Fujisaka T, Sui H, Suzuki RO. Design and numerical evaluation of cascade-type thermoelectric modules. J Electron Mater 2013;42(7):1688–96.
[10] Mahan GD. Inhomogeneous thermoelectrics. J Appl Phys 1991;70(8):4551–4.
[11] Schilz J, Helmers L, Muller WE, Niino M. A local selection criterion for the composition of graded thermoelectric generators. J Appl Phys 1998;83(2):1150–2.
[12] Muller E, Drasar C, Schilz J, Kaysser WA. Functionally graded materials for sensor and energy applications. Mat Sci Eng Struct 2003;362(1–2):17–39.
[13] Liu WS, Yan X, Chen G, Ren ZF. Recent advances in thermoelectric nanocomposites. Nano Energy 2012;1(1):42–56.
[14] Ioffe AF. Thermoelectric battery. SU Author's certificate No126158. 1960. Published in Invention Bulletin No.4.
[15] Ming T, Wu Y, Peng C, Tao Y. Thermal analysis on a segmented thermoelectric generator. Energy 2015;80:388–99.
[16] Snyder GJ. Application of the compatibility factor to the design of segmented and cascaded thermoelectric generators. Appl Phys Lett 2004;84(13):2436–8.
[17] Kuznetsov VL, Kuznetsova LA, Kaliazin AE, Rowe DM. High performance functionally graded and segmented Bi2Te3-based materials for thermoelectric power generation. J Mater Sci 2002;37(14):2893–7.
[18] Rowe DM. Thermoelectrics handbook : macro to nano. Boca Raton: CRC/Taylor & Francis; 2006.
[19] Dashevsky Z, Gelbstein Y, Edry I, Drabkin I, Dariel M. Optimization of thermoelectric efficiency in graded materials. Conference Optimization of thermoelectric efficiency in graded materials. IEEE, p. 421–424.
[20] Helmers L, Muller E, Schilz J, Kaysser WA. Graded and stacked thermoelectric generators - numerical description and maximisation of output power. Mat Sci Eng B Solid 1998;56(1):60–8.
[21] Yan XA, Poudel B, Ma Y, Liu WS, Joshi G, Wang H, et al. Experimental studies on anisotropic thermoelectric properties and structures of n-type Bi2Te2.7Se0.3. Nano Lett 2010;10(9):3373–8.
[22] Wu Y, Zuo L, Chen J, Klein J. A model to analyze the device level performance of thermoelectric generator. Energy 2016;115:591–603.
[23] Moizhes BY, Shishkin Y, Petrov A, Kolomoets L. Choice of optimal mode of operation of a cascade thermoelectric element. Sov Phys Tech Phys 1962;7(4).336-&.
[24] Hicks LD, Dresselhaus MS. Thermoelectric figure of merit of a one-dimensional conductor. Phys Rev B 1993;47(24):16631–4.
[25] Hicks LD, Dresselhaus MS. Effect of quantum-well structures on the

thermoelectric figure of merit. Phys Rev B 1993;47(19):12727–31.
[26] Snyder GJ, Toberer ES. Complex thermoelectric materials. Nat Mater 2008;7(2):105–14.
[27] Sootsman JR, Chung DY, Kanatzidis MG. New and old concepts in thermoelectric materials. Angew Chem Int Ed 2009;48(46):8616–39.
[28] Tan GJ, Zhao LD, Kanatzidis MG. Rationally designing high-performance bulk thermoelectric materials. Chem Rev 2016;116(19):12123–49.
[29] Zeier WG, Zevalkink A, Gibbs ZM, Hautier G, Kanatzidis MG, Snyder GJ. Thinking like a chemist: intuition in thermoelectric materials. Angew Chem Int Ed 2016;55(24):6826–41.
[30] Min G, Rowe DM. Recent concepts in thermoelectric power generation. In: Xxi international conference on thermoelectrics, proceedings Ict '02; 2002. p. 365–74.
[31] Huang MJ, Yen RH, Wang AB. The influence of the Thomson effect on the performance of a thermoelectric cooler. Int J Heat Mass Transf 2005;48(2):413–8.
[32] Lampinen MJ. Thermodynamic analysis of thermoelectric generator. J Appl Phys 1991;69(8):4318–23.
[33] Chen JC, Yan ZJ, Wu LQ. The influence of Thomson effect on the maximum power output and maximum efficiency of a thermoelectric generator. J Appl Phys 1996;79(11):8823–8.
[34] Al-Merbati AS, Yilbas BS, Sahin AZ. Thermodynamics and thermal stress analysis of thermoelectric power generator: influence of pin geometry on device performance. Appl Therm Eng 2013;50(1):683–92.
[35] Kraemer D, McEnaney K, Chiesa M, Chen G. Modeling and optimization of solar thermoelectric generators for terrestrial applications. Sol Energy 2012;86(5):1338–50.
[36] Chen G. Theoretical efficiency of solar thermoelectric energy generators. J Appl Phys 2011;109(10).
[37] Kumar S, Heister SD, Xu XF, Salvador JR, Meisner GP. Thermoelectric generators for automotive waste heat recovery systems Part I: numerical modeling and baseline model analysis. J Electron Mater 2013;42(4):665–74.
[38] Sahin AZ, Yilbas BS. The thermoelement as thermoelectric power generator: effect of leg geometry on the efficiency and power generation. Energy Convers Manag 2013;65:26–32.
[39] Ali H, Sahin AZ, Yilbas BS. Thermodynamic analysis of a thermoelectric power generator in relation to geometric configuration device pins. Energy Convers Manag 2014;78:634–40.
[40] Jang JY, Tsai YC, Wu CW. A study of 3-D numerical simulation and comparison with experimental results on turbulent flow of venting flue gas using thermoelectric generator modules and plate fin heat sink. Energy 2013;53:270–81.
[41] Snyder GJ, Ursell TS. Thermoelectric efficiency and compatibility. Phys Rev Lett 2003;91(14).
[42] Hu LP, Wu HJ, Zhu TJ, Fu CG, He JQ, Ying PJ, et al. Tuning multiscale microstructures to enhance thermoelectric performance of n-type Bismuth-telluride-based solid solutions. Adv Energy Mater 2015;5(17).
[43] Tang ZL, Hu LP, Zhu TJ, Liu XH, Zhao XB. High performance n-type bismuth telluride based alloys for mid-temperature power generation. J Mater Chem C 2015;3(40):10597–603.
[44] Duong AT, Nguyen VQ, Duvjir G, Duong VT, Kwon S, Song JY, et al. Achieving ZT=2.2 with Bi-doped n-type SnSe single crystals. Nat Commun 2016:7.
[45] Basu R, Bhattacharya S, Bhatt R, Roy M, Ahmad S, Singh A, et al. Improved thermoelectric performance of hot pressed nanostructured n-type SiGe bulk alloys. J Mater Chem A 2014;2(19):6922–30.
[46] Il Kim S, Lee KH, Mun HA, Kim HS, Hwang SW, Roh JW, et al. Dense dislocation arrays embedded in grain boundaries for high-performance bulk thermoelectrics. Science 2015;348(6230):109–14.
[47] Li YY, Li D, Qin XY, Yang XH, Liu YF, Zhang J, et al. Enhanced thermoelectric performance through carrier scattering at heterojunction potentials in BiSbTe based composites with Cu3SbSe4 nanoinclusions. J Mater Chem C 2015;3(27):7045–52.
[48] Tan GJ, Shi FY, Hao SQ, Zhao LD, Chi H, Zhang XM, et al. Non-equilibrium processing leads to record high thermoelectric figure of merit in PbTe-SrTe. Nat Commun 2016:7.
[49] Fu CG, Bai SQ, Liu YT, Tang YS, Chen LD, Zhao XB, et al. Realizing high figure of merit in heavy-band p-type half-Heusler thermoelectric materials. Nat Commun 2015:6.
[50] Harman TC, Honig JM. Thermoelectric and thermomagnetic effects and applications. 1967. 377 P MCGRAW-HILL INC, NEW YORK, N Y$ 17 50. 1967.
[51] Cohen R, Abeles B. Efficiency calculations of thermoelectric generators with temperature varying parameters. J Appl Phys 1963;34(6):1687–8.
[52] Rowe DM. CRC handbook of thermoelectrics. CRC press; 1995.
[53] El-Desouky A, Carter M, Mahmoudi M, Elwany A, LeBlanc S. Influences of energy density on microstructure and consolidation of selective laser melted bismuth telluride thermoelectric powder. J Manuf Process 2017;25:411–7.
[54] Kinemuchi Y, Mikami M, Terasaki I, Shin W. Rapid synthesis of thermoelectric compounds by laser melting. Mater Des 2016;106:30–6.
[55] El-Desouky A, Carter M, Andre MA, Bardet PM, LeBlanc S. Rapid processing and assembly of semiconductor thermoelectric materials for energy conversion devices. Mater Lett 2016;185:598–602.
[56] Mao Y, Yan YG, Wu KP, Xie HY, Xiu ZK, Yang JH, et al. Non-equilibrium synthesis and characterization of n-type Bi2Te2.7Se0.3 thermoelectric material prepared by rapid laser melting and solidification. RSC Adv 2017;7(35):21439–45.
[57] Harman TC, Taylor PJ, Walsh MP, LaForge BE. Quantum dot superlattice thermoelectric materials and devices. Science 2002;297(5590):2229–32.
[58] Nishio K, Hirano T. Improvement of the efficiency of thermoelectric energy conversion by utilizing potential barriers. Jpn J Appl Phys 1997;36(1a):170–4.1.
[59] Wang SY, Yang J, Toll T, Yang JH, Zhang WQ, Tang XF. Conductivity-limiting bipolar thermal conductivity in semiconductors. Sci Rep Uk 2015:5.
[60] Chen G. Nanoscale energy transport and conversion: a parallel treatment of electrons, molecules, phonons, and photons. Oxford; New York: Oxford University Press; 2005.